UC San Diego
UC San Diego Previously Published Works

Title
MAGNETIC AND DENSITY SPIKES IN COSMIC-RAY SHOCK PRECURSORS

Permalink
https://escholarship.org/uc/item/6fg512hd

Journal
The Astrophysical Journal Letters, 748(2)

ISSN
2041-8205

Authors
Malkov, MA
Sagdeev, RZ
Diamond, PH

Publication Date
2012-04-01

DOI
10.1088/2041-8205/748/2/l32

Peer reviewed

MAGNETIC AND DENSITY SPIKES IN COSMIC-RAY SHOCK PRECURSORS

M. A. MALKOV[1], R. Z. SAGDEEV[2], AND P. H. DIAMOND[1,3]
[1] CASS and Department of Physics, University of California, San Diego, La Jolla, CA 92093, USA; mmalkov@ucsd.edu
[2] Department of Physics, University of Maryland, College Park, MD 20742-3280, USA
[3] WCI Center for Fusion Theory, National Fusion Research Institute, Gwahangno 113, Yuseong-gu, Daejeon 305-333, Republic of Korea

ABSTRACT

In shock precursors populated by accelerated cosmic rays (CRs), the CR return current instability is believed to significantly enhance the pre-shock perturbations of magnetic field. We have obtained *fully nonlinear* exact ideal MHD solutions supported by the CR return current. The solutions occur as localized spikes of circularly polarized Alfvén envelopes (solitons or breathers). As the conventional (undriven) solitons, the obtained magnetic spikes propagate at a speed C proportional to their amplitude, $C = C_A B_{\max}/\sqrt{2} B_0$. The sufficiently strong solitons run thus ahead of the main shock and stand in the precursor, being supported by the return current. This property of the nonlinear solutions is strikingly different from the linear theory that predicts non-propagating (that is, convected downstream) circularly polarized waves. The nonlinear solutions may come either in isolated pulses (solitons) or in soliton-trains (cnoidal waves). The morphological similarity of such quasi-periodic soliton chains with recently observed X-ray stripes in the Tycho supernova remnant (SNR) is briefly discussed. The magnetic field amplification determined by the suggested saturation process is obtained as a function of decreasing SNR blast wave velocity during its evolution from the ejecta dominated to the Sedov–Taylor stage.

Key words: acceleration of particles – cosmic rays – ISM: magnetic fields – ISM: supernova remnants – magnetohydrodynamics (MHD) – shock waves

Online-only material: color figure

1. INTRODUCTION

The nonresonant cosmic-ray (CR) return current instability (also termed as Bell's instability) is expected to bootstrap the acceleration of CR in shocks by enhancing the magnetic field in the shock precursor. The most unstable is a circularly polarized, field-aligned, aperiodic mode, similar to the internal kink (Kruskal-Shafranov) mode in plasmas (see, e.g., Ryutov et al. 2006). Regarding the CR acceleration in shocks, it was studied by Achterberg (1983) and Shapiro et al. (1998).

Bell (2004) reawakened the interest in this instability by emphasizing its role in magnetic field amplification and suggested its saturation due to magnetic tension. However, since the growth rate decreases with the wavenumber only as $\sqrt{k}$, the magnetic tension is insufficient to stabilize long waves. This opens the door for a strong, $\delta B \gg B_0$ field amplification. The caveat is that the non-propagating long waves have limited (precursor-crossing) time to grow. By contrast, the nonlinear solutions, obtained in this Letter, can stand off ahead of the shock, thus warranting the saturation.

Studies of the Bell's mode saturation mechanisms are primarily based on the magnetohydrodynamic (MHD) and particle-in-cell simulations (Bell 2004; Pelletier et al. 2006; Vladimirov et al. 2006; Reville et al. 2007; Niemiec et al. 2008; Zirakashvili et al. 2008; Bykov et al. 2009; Luo & Melrose 2009; Riquelme & Spitkovsky 2009; Stroman et al. 2009; Dieckmann et al. 2010). As demonstrated in a three-dimensional (3D) MHD simulation by Bell (2005; see also Niemiec et al. 2008), the saturation is achieved when the Ampère force expels plasma and the helical magnetic field radially, thus forming plasma cavities. The instability saturates only in 3D, or at least in quasi-two-dimensional (2D) dynamics, perpendicular to the ambient field. However, the fastest growing modes are field-aligned, i.e., initially one dimensional (1D). Therefore, it is necessary to understand structures that form at the 1D phase and particularly the nonlinear mechanisms of their saturation and propagation ahead of the shock. These structures may in the main cease to grow by spreading the saturated turbulence energy in k-space before the subsequent 3D dynamics kick in. Although this scenario may appear to be at odds with many simulations, recent *Chandra* observations of the Tycho supernova remnant (SNR), for example, indicate the presence of quasi-1D structures (stripes), inconsistent with the quasi-isotropic nonlinear dynamics observed in those simulations (Eriksen et al. 2011). Moreover, while being very useful for our understanding of CR instabilities, simulations cover only a tiny fraction of the dynamical range of typical SNR-shock acceleration process and introduce artificial dissipation in collisionless plasmas.

Alfvén waves usually saturate by modulational instability. However, being a strong MHD *aperiodic* instability, Bell's instability hampers direct applications of standard methods, such as the weak-turbulence theory (Sagdeev & Galeev 1969). The latter typically deals with propagating and weakly interacting eigen modes and, as a driver amplifies them, they cascade the wave energy to the dissipation scale. The Bell's linear mode does not propagate and does not even exist without the driving current. The lack of long-wave stabilization is seen from the comparison of linear contributions to the square of the growth rate of the driving current ($\propto k$) and magnetic tension ($\propto k^2$, Equation (12) below). A clue to saturation in a similar system of the pressure-anisotropy-driven fire-hose instability is provided by an exact solution due to Berezin & Sagdeev (1969). While peak magnetic energy takes nearly all the instability free energy ($B_\perp^2/8\pi \sim P_\parallel - P_\perp \gg B_0^2/8\pi$), on the average only the moderate field amplification $B_\perp \sim B_0$ is observed.

In this Letter, we present an exact solution of the *current-driven* MHD equations (e.g., CR return current). It differs from the linearly growing solution in that it propagates

with the velocity proportional to its (constant) amplitude and is spatially localized.

2. BASIC EQUATIONS

The linear theory of Bell's instability indicates that the fastest-growing modes are field-aligned (Bell 2005). Therefore, we consider 1D MHD equations in a CR shock precursor using a coordinate system with the axis x along the field. The general 1D equations read

$$\frac{d\rho}{dt} + \rho \frac{\partial}{\partial x} U_x = 0, \qquad (1)$$

$$\frac{dU_x}{dt} = -\frac{1}{\rho} \frac{\partial}{\partial x} \frac{B_\perp^2}{8\pi}, \qquad (2)$$

$$\frac{d\mathbf{U}_\perp}{dt} = \frac{B_0}{4\pi\rho} \frac{\partial \mathbf{B}_\perp}{\partial x} + \frac{1}{c\rho} \mathbf{J} \times \mathbf{B}_\perp, \qquad (3)$$

$$\frac{d\mathbf{B}_\perp}{dt} = B_0 \frac{\partial \mathbf{U}_\perp}{\partial x} - \mathbf{B}_\perp \frac{\partial U_x}{\partial x}. \qquad (4)$$

Here $d/dt \equiv \partial/\partial t + U_x \partial/\partial x$, ρ is the gas density, U_x, B_0 and $\mathbf{U}_\perp$, $\mathbf{B}_\perp$ are the gas velocity and magnetic field components along the field (x-direction) and in the (y, z)-plane, respectively. The x-component of the magnetic field $B_x = B_0 = $ constant because of $\nabla \cdot \mathbf{B} = \mathbf{0}$. In Equation (3), we have included the plasma return current by representing the total plasma current as $\mathbf{J}_{tot} = (c/4\pi)\nabla \times \mathbf{B} + \mathbf{J}$, where the term $\mathbf{J} = -\mathbf{J}_{CR}$ compensates the CR current. Equation (3) implies that in our reference frame $\mathbf{J} \times \mathbf{B}_0 = 0$. We neglect the thermal and CR pressure, as Bell (2004) did. It should be noted, however, that the CR pressure gradient drives an acoustic instability of the shock precursor (also called Drury's instability, Drury 1984; Dorfi 1984). Moreover, the acoustic instability grows faster than the Bell's instability for $\beta = 8\pi P/B_0^2 < 1$ (see Malkov et al. 2010 where the studies of evolution, saturation, associated particle transport, and cascading of magnetic energy are also referenced).

Returning to Equations (1)–(4), we introduce a Lagrangian mass coordinate ξ:

$$d\xi = \frac{\rho}{\rho_0}(dx - U_x dt), \qquad (5)$$

where ρ_0 is the background density. Considering scales shorter than the precursor size, we treat ρ_0 and the bulk plasma speed U_{x0} as coordinate independent ($U_{x0} = 0$ in the plasma frame).

Next, we reduce Equations (1)–(4) to the following system of two equations that describe the magnetic field and density perturbations:

$$\frac{\partial^2}{\partial t^2} \frac{B}{\rho} - C_A^2 \frac{\partial^2}{\partial \xi^2} \frac{B}{\rho_0} = \frac{i}{c\rho_0} B_0 J \frac{\partial}{\partial \xi} \frac{B}{\rho} \qquad (6)$$

$$\frac{\partial^2}{\partial t^2} \frac{\rho_0^2}{\rho} + \frac{\partial^2}{\partial \xi^2} \frac{|B|^2}{8\pi} = 0, \qquad (7)$$

where

$$B = B_y + iB_z \quad \text{and} \quad C_A^2 = \frac{B_0^2}{4\pi\rho_0}.$$

The right-hand side of Equation (6) is the instability driver. Without it, the equations describe the conventional MHD modes,

propagating at an angle $\vartheta = \tan^{-1}(|\bar{B}|/B_0)$ to the ambient magnetic field. By choosing the averaged components $\overline{B}_y = \overline{B}_z = 0$, we restrict our treatment to the parallel propagation along the x-direction.

3. TRAVELING WAVE SOLUTIONS

We look for the solutions of the system given by Equations (6) and (7) in the form of a traveling wave:

$$B = B_{max} v(\zeta)e^{-i\omega t} \qquad (8)$$

$$\rho = \rho(\zeta),$$

where $\zeta = \xi - Ct$, C is the (constant) propagation speed of the traveling wave, B_{max} is the wave amplitude that we specify in Equation (9) below, and $\omega = \Re\omega$ is the wave frequency. Note that for $\omega \neq 0$, the solution is not steady in any reference frame. A spatially localized solution is usually called "breather" as opposed to the soliton, customary to $\omega = 0$ case. Integrating then Equation (7) twice, we obtain

$$\frac{\rho_0}{\rho} = 1 - \frac{|B|^2}{B_{max}^2}, \qquad (9)$$

where $B_{max}^2 \equiv 8\pi\rho_0 C^2$. We have chosen the integration constants in such a way that $B \to 0$ for $\rho \to \rho_0$ (background plasma) and $B \to B_{max}$ for $\rho \to \infty$ (flow stagnation point, if present). This sets the interval for variation of $v(\zeta)$: $0 < v < 1$.

Substituting B from Equation (8) and ρ from the last equation, Equation (6) yields

$$\frac{\partial^2}{\partial \zeta^2}(a - |v|^2)v - iK\frac{\partial}{\partial \zeta}(1 - |v|^2)v - \frac{\omega^2}{C^2}(1 - |v|^2)v = 0. \quad (10)$$

Here, we have used the following notations

$$K = \frac{B_0 J}{c\rho_0 C^2} - 2\frac{\omega}{C}, \quad a = 1 - 2\frac{B_0^2}{B_{max}^2} = 1 - \frac{C_A^2}{C^2}, \qquad (11)$$

where $C_A^2 = B_0^2/4\pi\rho_0$. The linear dispersion relation can be recovered by letting $v(\zeta) \propto e^{ik\zeta}$, $v \to 0$ in Equation (10):

$$\omega = kC \pm \sqrt{k^2 C_A^2 + B_0 Jk/c\rho_0}. \qquad (12)$$

The arbitrary propagation speed C is a parameter of a Galilean transformation (zero in the plasma frame), while the imaginary part of ω is an invariant of such transformation, as it should be. In the nonlinear treatment, the wave velocity with respect to the plasma depends on the wave amplitude (nonlinear dispersion relation). Meanwhile, the linear instability occurs in the long-wave limit for $-B_0^2 J^2/c\rho_0 C_A^2 < B_0 Jk < 0$, for the polarization chosen in Equation (6). It should be emphasized that only if the quadratic B term is neglected in Equation (9), is there no coupling to the density modulations in Equation (6). It is interesting to note that in the strong nonlinear limit $B_{max}/B_0 \to \infty$, Equation (10) degenerates into a linear equation for the function $v(1 - |v|^2)$. This limit, however, cannot be understood without the nonlinear solution.

To find such solution, we write

$$v(\zeta) = \sqrt{w}e^{i\Theta}, \qquad (13)$$

where $w(\zeta) \geqslant 0$. Substituting v from Equation (13) into Equation (10) and separating the imaginary part, for the phase Θ we obtain the following equation:

$$\frac{d\Theta}{ds} = \frac{wP(w) + A}{w(a - w)^2}, \quad (14)$$

where

$$P \equiv w^2 - (3a + 1)w/2 + a.$$

We have introduced a new variable $s = K\zeta/2$ and an integration constant A. We may choose it by specifying the properties of the solution sought. The regularity of Θ at $w = 0$ implies $A = 0$. Next, taking the real part of Equation (10) and using Equation (14) with $A = 0$, for $w(s)$ we obtain

$$\frac{d^2 f}{ds^2} - \frac{w^2 P^2}{f^3} + 2\sqrt{w}(1 - w)\left[\frac{wP}{f^2} - 2\frac{\omega^2}{C^2 K^2}\right] = 0, \quad (15)$$

where we have denoted

$$f(w) \equiv \sqrt{w}(a - w).$$

Equation (15) can be readily integrated by multiplying it by df/ds. We choose the integration constant to select an isolated pulse (soliton) solution of Equation (15), i.e., $w \to 0$, as $s \to \pm\infty$. Then, the first integral reads

$$\left(\frac{dw}{ds}\right)^2 - \frac{w^2}{(3w - a)^2(a - w)^2}\sum_{n=0}^{4} C_n w^n = 0, \quad (16)$$

where

$$
\begin{aligned}
C_0 &= & 4a^2(a\mu^2 - 1) \\
C_1 &= & 2a[2(3 + a) - a\mu^2(7 + a)] \\
C_2 &= & 8\mu^2 a(a + 2) - a^2 - 14a - 9 \\
C_3 &= & 2[2(3 + a) - \mu^2(3 + 5a)] \\
C_4 &= & 4(\mu^2 - 1)
\end{aligned}
$$

with

$$\mu^2 \equiv 4\omega^2/K^2 C^2 = \left(1 - \frac{B_0 J}{2c\rho_0 C\omega}\right)^{-2}.$$

A useful analogy between nonlinear waves and nonlinear oscillators (e.g., Sagdeev 1966) suggests interpreting the first term (Equation (16)) as kinetic and the second term as potential energy. The "oscillator's coordinate" $w > 0$, as a function of "time" s, leaves $w = 0+$ at $s = -\infty$ and returns there at $s = +\infty$. *Periodic* solutions (cnoidal waves) can also be easily found by changing the integration constant.

The amplitude $w_0(a, \mu)$ of the localized solution (soliton) is obviously determined by the smallest positive root of the polynomial in Equation (16), so that the "oscillator" bounces between $w = 0$ and $w = w_0$. In the simplest case of a small amplitude solution

$$w_0 \approx -C_0/C_1 \ll a < 1$$

(where $C_0 > 0$ and $C_1 < 0$), the solution has a classical soliton profile:

$$w(s) = \frac{w_0}{\cosh^2\left(\frac{\sqrt{C_0}}{2a^2}s\right)}. \quad (17)$$

Apart from the condition $a\mu^2 > 1$ (to ensure $w_0 > 0$), i.e.,

$$1 - \sqrt{1 - C_A^2/C^2} < \frac{B_0 J}{2c\rho_0\omega C} < 1 + \sqrt{1 - C_A^2/C^2}$$

and the technical restriction $a\mu^2 - 1 \ll 1$ (to neglect the $n > 1$ terms in Equation (16)), this solution imposes no further constraints on ω and C. However, it has a very strong amplitude limitation, $a\mu^2 - 1 \ll 1$ (virtually a wave packet of linear waves). We are interested in an opposite case of highly super-Alfvénic solitons that are not convected rapidly with the flow into the subshock and may stay ahead of it, when $C \gg C_A$.

A relation between ω and C (nonlinear dispersion relation) arises from the extension of the above solution to larger w_0. Clearly, we have to pass the point $w = a/3$ smoothly which requires a double root of the polynomial in Equation (16) at $w = a/3$:

$$\sum_{n=0}^{4} C_n \left(\frac{a}{3}\right)^n = \sum_{n=1}^{4} nC_n \left(\frac{a}{3}\right)^{n-1} = 0.$$

Interestingly, the both conditions are met simultaneously as soon as the following dispersion relation is satisfied:

$$a\mu^2 = \frac{9 - a}{8}. \quad (18)$$

Recalling that the small amplitude soliton $w_0 \ll 1$ branches off from the trivial solution at the threshold $a\mu^2 = 1$, in the case of $C_A \ll C$, i.e., $a \approx 1$, we may accept Equation (18) to be valid in the entire parameter range $a\mu^2 > 1$.

Let us rewrite the above dispersion relation as follows:

$$\omega = \frac{k_J C}{M_A^2 \left(1 \pm \sqrt{\left(1 - M_A^{-2}\right)/\left(1 + 1/8M_A^2\right)}\right)},$$

where we have defined the instability wavenumber (see Equation (12)) as $k_J = 2\pi J/cB_0$. Strong solitons with $M_A \equiv C/C_A \gg 1$ have either high or low frequency: $\omega = (16/9)k_J C$, $\omega = k_J C/2M_A^2$. The spatial scale of the solitons is given by its "wavenumber" K, Equation (11), Figure 1:

$$K = \pm\frac{2k_J}{M_A^2}\frac{\sqrt{\left(1 - M_A^{-2}\right)/\left(1 + 1/8M_A^2\right)}}{1 \pm \sqrt{\left(1 - M_A^{-2}\right)/\left(1 + 1/8M_A^2\right)}}. \quad (19)$$

Both solutions disappear (spread to infinity) in the limit $J \to 0$, although they have disparate scales, particularly for $M_A \gg 1$. Therefore, the external current is essential and there is no transition to conventional simple wave MHD solutions for the vanishing CR current.

To obtain the spatial structure of the above solutions, we substitute Equation (18) into Equation (16). The latter takes the following simple form:

$$\left(\frac{dw}{ds}\right)^2 = \frac{1 - a}{2a}\frac{w^2}{(a - w)^2}Q^2(w), \quad (20)$$

where

$$Q^2 \equiv w^2 - 2hw + a; \quad h = (a + 3)/4.$$

Equation (20) can be reduced to a quadrature:

$$s(w) = \sqrt{\frac{2a}{1 - a}}\left[\cosh^{-1}\frac{h - w}{\sqrt{h^2 - a}} + \sqrt{a}R\right], \quad (21)$$
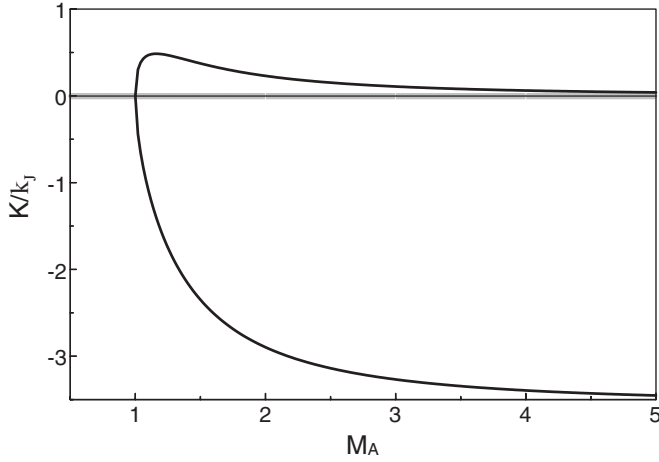
Figure 1. Dispersive properties of the two types of solitons: the short scale (lower branch) and the long scale (upper brunch). The soliton wavenumber K is shown in the units of $k_J = 2\pi J/cB_0$, as a function of $M_A = C/C_A$. For the parameter values of interest, the CR current-carrying particles have gyroradii $r_g k_J \sim 10^3$ (Bell 2004) which must also be larger than the soliton scale K^{-1}, $Kr_g \gtrsim 1$ (to justify the fixed J approximation). Obviously, this restriction (schematically shown by shaded area near abscissa) affects only the long-wave soliton and translates into $M_A^2 < k_J r_g$ requirement (see also Section 5).
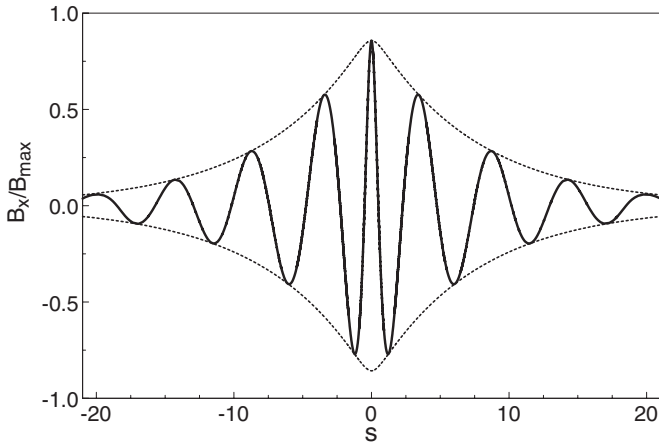

Figure 2. B_x-component of the soliton solution as a function of dimensionless coordinate $s = K\zeta/2$ in units of $B_{\max}$ ($B_{\max}^2 \equiv 8\pi\rho_0 C^2$): $B_x/B_{\max} = \sqrt{w}\cos(\Theta)$ shown with the solid line and the amplitude envelope, $\pm\sqrt{w}$ (dashed line). The soliton Mach number $M_A = C/C_A = 3$ corresponds to the amplitude parameter $a = 1 - M_A^{-2} = 8/9$.

where

$$R = \ln\frac{\sqrt{a} + w - Q}{\sqrt{a} - w + Q} - \ln\frac{\sqrt{a} - \sqrt{h^2 - a} + h}{\sqrt{a} + \sqrt{h^2 - a} - h}.$$

Using Equations (14) and (20), the solution for the phase $\Theta(w)$ can be reduced to another quadrature

$$\Theta = \sqrt{\frac{2a}{1-a}}\left[\cosh^{-1}\frac{h-w}{\sqrt{h^2 - a}} + R/\sqrt{a}\right]$$
$$- 2\left[\tan^{-1}\left(\frac{Q - w + a}{\sqrt{a(1-a)/2}}\right) - \tan^{-1}\left(\frac{\sqrt{h^2 - a} - h + a}{\sqrt{a(1-a)/2}}\right)\right].$$
$$(22)$$

The B_x-component of the solitary solution is shown in Figure 2 (the $e^{-i\omega t}$-factor omitted). The wave packet in the compressed area becomes more oscillatory, as may also be seen
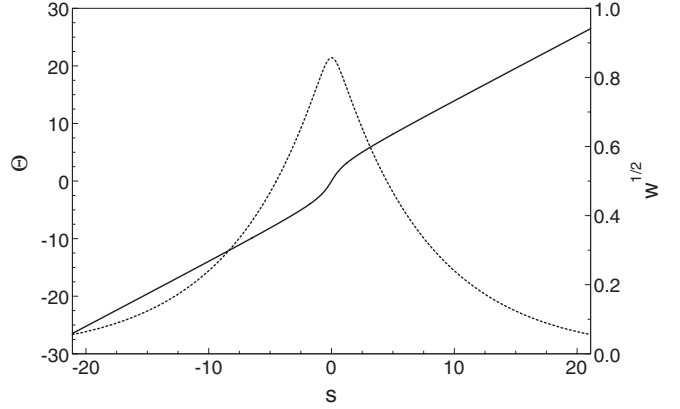

Figure 3. Phase Θ as a function of coordinate s, shown with the solid line. The amplitude of the soliton is shown with the dashed line.

from Figure 3, which shows the soliton phase Θ as a function of dimensionless coordinate s. The local dimensionless wavenumber stays approximately constant ($d\Theta/ds \approx 1$), apart from the above phase steepening near the maximum amplitude, where $d\Theta/ds \approx 2$.

4. MAXIMUM MAGNETIC FIELD

The isolated solitons obtained in this Letter belong to a one-parameter family; the amplitude $B_{\max}$ or Mach number $M_A = B_{\max}/\sqrt{2}B_0$ can be used as such a parameter. In a CR shock precursor, the soliton scale may be determined by the scale of seed waves for the subsequent *nonresonant* instability. The seed waves may be *resonantly* excited upstream of the strong CR current zone by the high-energy CRs. Then, $K \sim r_g^{-1}(p_*)$, where r_g is the gyroradius of the seed-generating CRs of momentum $p = p_*$. This amounts to $M_A^2 = k_J r_g(p_*)$ for the upper (long-wave, Figure 1) soliton branch in Equation (19). Note that p_* may be $\ll p_{\max}$ due to a poor CR confinement in the range $p_* < p < p_{\max}$ (Malkov & Diamond 2006), so that the $Kr_g \gtrsim 1$ requirement, to justify the formal $J_{CR} = -J \approx$ constant assumption, is still met for $p > p_*$.

If the CR current is sufficiently strong, $k_J r_g(p_*) \gg 1$ and only the upper-sign soliton in Equation (19) and Figure 1 can accommodate the requirement $K \sim r_g^{-1}(p_*)$ for $M_A \gg 1$. Then, the maximum magnetic field for a given soliton can be written as $B_{\max}^2/B_0^2 = 2M_A^2 \approx 2k_J r_g(p_*)$, or

$$B_{\max}^2 = 4\pi V_s n_{CR} p_*, \qquad (23)$$

where n_{CR} is the CR density.

The scaling of CR-enhanced magnetic energy with the ambient density ρ and shock velocity V_s is debated in the literature. Bell (2004) suggested $B^2/\rho \propto V_s^3$, whereas Völk et al. (2005) indicate that $B^2/\rho \propto V_s^2$. The difference between the two scalings is whether a fraction of *mechanical energy flux* or *momentum flux* goes into magnetic energy. By contrast, Equation (23) constitutes the conversion of *CR energy flux* into magnetic energy. Vink (2008) summarizes the information about the magnetic field from a number of SNR, with the two phenomenological scalings superimposed, Figure 4. Note that $B_{\max}$ in Equation (23) coincides with the condition of magnetization (trapping by the wave) of the current-carrying particles $k_J(B_{\max})r_g(p_*, B_{\max}) = 1/2$, which is also (formally) similar to the Bell's phenomenological condition of balancing the Ampère force and the magnetic tension for the instability saturation.
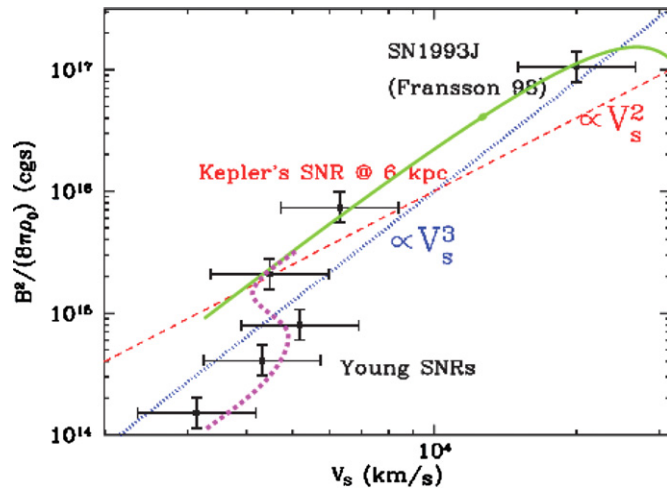
Figure 4. Ratio of the magnetic field energy to ambient density ρ_0 as a function of shock velocity V_s adopted from (Vink 2008; points with error bars). The blue dotted line is the scaling from Bell (2004), while the red dashed line is that of Völk et al. (2005), both also taken from the Vink's compilation. An example of calculations, described in Section 4, is shown with the green line. The field energy declines beyond $V_s \approx 2.7 \times 10^4$ to vanish at $V_0 \approx 9 \times 10^4$ km s^{-1} (not shown in the plot). At lower V_s, where the shock acceleration is inefficient, this dependence breaks down and should transition to a low-efficiency acceleration regime in a bistable fashion (Drury & Voelk 1981; Malkov 1997; schematically shown with the magenta dotted line).

(A color version of this figure is available in the online journal.)

However, the saturation mechanism behind Equation (23) is different in that $B_{\max}$ is only the peak magnetic field. The magnetic energy density would be smaller by a soliton filling factor (cf. Berezin & Sagdeev 1969). More importantly, the efficiency of CR acceleration and subsequent conversion of their energy into magnetic field should depend on J, V_s, and other acceleration parameters which almost certainly rules out the single power-law relation between B^2/ρ and V_s.

Therefore, we obtain such relation in a different way, which we outline below and will describe in detail elsewhere. Consider a nominal SNR with the shock speed V_s slowing down from an initial $V_s = V_0 = 1.34 \times V_{ST}$ to $V_s \approx 0.1 \times V_0$ (i.e., well into the Sedov–Taylor phase), where $V_{ST} = 10{,}400 \times E_{51}^{1/2}(M_e/M_\odot)^{1/2}$ km s^{-1} (McKee & Truelove 1995). Here E_{51} is the explosion energy in 10^{51} erg and M_e is the ejecta mass. During its evolution, the SNR should follow the points sampled from a set of supposedly similar remnants in Figure 4. Using the $V_s(t)$ dependence from McKee & Truelove (1995) and the momentum $p_* \sim p_{\max}(t)$ in the nonlinear acceleration regime from Malkov & Drury (2001, Equation (7.45)), we express p_* in Equation (23) as a function of V_s. Next, we obtain n_{CR} from Equation (15) in Malkov (1997) for the evolving subshock strength with the particle injection rate held approximately constant in the efficient acceleration regime (see Equation (37) in the same reference). Using these results, we finally obtain from Equation (23) an expression for $B_{\max}^2/\rho$, again, as a function of V_s. A preliminary example of such calculation is shown in Figure 4 with the green line. In an intermediate range of V_s, the scaling is $\propto B_m^2/\rho \propto V_s^{11/4}$ (close to the Bell's scaling) but it rolls over to turn to zero at $V_s = V_0 \approx 9 \times 10^4$ km s^{-1}. This is because the magnetic field generation is pinned to the CRs (Equation (23)) which are not yet there at $V_s = V_0$, i.e., at $t = 0$. The other strong deviation from a power law should occur at lower V_s where acceleration bifurcates into an inefficient (test particle) regime through a characteristic S-curve (Malkov 1997).

5. DISCUSSION

The purpose of this Letter was to understand the nonlinear evolution of the nonresonant current-driven instability by studying saturated nonlinear waves (solitons). They (or their shock counterparts, if dissipation is efficient) may comprise the asymptotic state of the system. Such a scenario is supported by simpler (but fully integrable, e.g., Kaup & Newell 1978) weakly nonlinear MHD models, such as the derivative nonlinear Schroedinger equation (see also Mjolhus & Hada 1997 for a review). In such models, arbitrary initial conditions evolve into an asymptotic state of quasi-independently propagating solitons, similar to those found in the present Letter. The difference, however, is that our system is current driven and its solutions have no MHD analogues.

The relevant question of soliton stability should be addressed in 2D–3D setting. The 2D–3D instability of a 1D soliton could comprise a wave front self-focusing (Passot & Sulem 2003) and thus elucidate the subsequent 3D structures. Such studies are beyond the scope of this letter, but a qualitative stability criterion may be suggested by the nonlinear dispersion relation given by Equation (19) and Figure 1. The parts of the dispersion curves with $\partial|K|/\partial C < 0$ (where K and $C \propto M_A$ are the wavenumber and propagation speed) correspond to the solitons with negative dispersion and should be stable. The oft-used justification of this criterion is that a nonlinear steepening of the soliton's leading edge generates higher wavenumber modes and they should not run faster than the soliton itself (negative dispersion is thus required). It should also be noted here that, once the soliton solutions of the driven system are obtained, they can also be arranged in a quasi-periodic or even chaotic soliton lattice. By adding a weak dissipation, the leading edges of these solitons can be converted into shock fronts (Sagdeev 1966) which usually increases the dissipation of the driver energy, thus reducing the saturation amplitude.

There exists upper bound on $B_{\max}$ since solitons with $C/C_A = B_{\max}/\sqrt{2}B_0 > V_s/C_A$ outrun the shock and cannot be sustained by the return current (soliton standing in the flow requires $C = V_s$). However, as *transients,* they may promote particle acceleration far upstream to synergistically supply themselves with the CR return current. This might be a plausible scenario for much-discussed CR acceleration bootstrap (e.g., Blandford & Funk 2007). In addition, the solitons may lead to shock reformation by initiating a new shock upstream. A seemingly analogous phenomenon was recently observed in PIC simulations by Gargaté & Spitkovsky (2012). Furthermore, strong solitons running ahead of the shock may become visible in X-rays as quasi-periodic stripes, similar to those recently observed in some parts of the Tycho SNR by *Chandra* (Eriksen et al. 2011). The identification of the stripe spacing with the maximum gyroradius of accelerated particles is consistent also with our determination of the soliton spacing in Section 4. The scale is set by the highest energy particles ahead of the field amplification zone. The soliton wave length, however, should be noticeably shorter than the distance between them. At the same time, similar structures may result from the nonlinear evolution of the CR-pressure-driven acoustic instability (Malkov & Diamond 2009), or shock front rippling (Mond & O'C. Drury 1998). Both the Drury's and Bells's instabilities (after adding dissipation to the soliton solution) should result in considerably shorter nonlinear shock structures than the conventional CR precursor of the standard Bohm diffusion model (Malkov et al. 2010). The magnetic field enhancement is likely to be weaker in the acoustic case, if it is merely due to the individual shock compression in the

instability-generated shock-train, without subsequent vorticity (and thus magnetic field) generation by interacting shocks (Samtaney & Zabusky 1994). Alternative approaches to the explanation of the recent *Chandra* observations (Eriksen et al. 2011) have also been suggested (Bykov et al. 2011; Rakowski et al. 2011). In conclusion, the proposed mechanism of the current-driven instability saturation is also interesting in that it introduces such fascinating and ubiquitous objects as solitons (e.g., Ablowitz & Segur 1981) to SNR physics. However, the dominant instability should be selected on a case-by-case basis by considering the alternatives in a given shock environment.

REFERENCES

Ablowitz, M. J., & Segur, H. (ed.) 1981, Solitons and the inverse scattering transform (Philadelphia: SIAM)
Achterberg, A. 1983, A&A, 119, 274
Bell, A. R. 2004, MNRAS, 353, 550
Bell, A. R. 2005, MNRAS, 358, 181
Berezin, Y. A., & Sagdeev, R. Z. 1969, Sov. Phys. Dokl., 14, 62
Blandford, R., & Funk, S. 2007, in AIP Conf. Ser. 921, The First GLAST Symposium, ed. S. Ritz, P. Michelson, & C. A. Meegan (Melville, NY: AIP), 62
Bykov, A. M., Ellison, D. C., Osipov, S. M., Pavlov, G. G., & Uvarov, Y. A. 2011, ApJ, 735, L40
Bykov, A. M., Osipov, S. M., & Toptygin, I. N. 2009, Astron. Lett., 35, 555
Dieckmann, M. E., Murphy, G. C., Meli, A., & Drury, L. O. C. 2010, A&A, 509, A89
Dorfi, E. 1984, Adv. Space Res., 4, 205
Drury, L. O. 1984, Adv. Space Res., 4, 185
Drury, L. O., & Voelk, J. H. 1981, ApJ, 248, 344
Eriksen, K. A., Hughes, J. P., Badenes, C., et al. 2011, ApJ, 728, L28
Gargaté, L., & Spitkovsky, A. 2012, ApJ, 744, 67
Kaup, D. J., & Newell, A. C. 1978, J. Math. Phys., 19, 798
Luo, Q., & Melrose, D. 2009, MNRAS, 397, 1402
Malkov, M. A. 1997, ApJ, 491, 584
Malkov, M. A., & Diamond, P. H. 2006, ApJ, 642, 244
Malkov, M. A., & Diamond, P. H. 2009, ApJ, 692, 1571
Malkov, M. A., Diamond, P. H., & Sagdeev, R. Z. 2010, Plasma Phys. Control. Fusion, 52, 124006
Malkov, M. A., & Drury, L. O. 2001, Rep. Prog. Phys., 64, 429
McKee, C. F., & Truelove, J. K. 1995, Phys. Rep., 256, 157
Mjolhus, E., & Hada, T. 1997, in Nonlinear Waves and Chaos in Space Plasmas, ed. T. Hada & H. Matsumoto (Tokyo: Terra Scientific Publishing), 121
Mond, M., & O'C. Drury, L. 1998, A&A, 332, 385
Niemiec, J., Pohl, M., Stroman, T., & Nishikawa, K.-I. 2008, ApJ, 684, 1174
Passot, T., & Sulem, P. L. 2003, Phys. Plasmas, 10, 3914
Pelletier, G., Lemoine, M., & Marcowith, A. 2006, A&A, 453, 181
Rakowski, C. E., Laming, J. M., Hwang, U., et al. 2011, ApJ, 735, L21
Reville, B., Kirk, J. G., Duffy, P., & O'Sullivan, S. 2007, A&A, 475, 435
Riquelme, M. A., & Spitkovsky, A. 2009, ApJ, 694, 626
Ryutov, D. D., Furno, I., Intrator, T. P., Abbate, S., & Madziwa-Nussinov, T. 2006, Phys. Plasmas, 13, 032105
Sagdeev, R. Z. 1966, Rev. Plasma Phys., 4, 23
Sagdeev, R. Z., & Galeev, A. A. 1969, Nonlinear Plasma Theory (New York: Benjamin)
Samtaney, R., & Zabusky, N. J. 1994, J. Fluid Mech., 269, 45
Shapiro, V. D., Quest, K. B., & Okolicsanyi, M. 1998, Geophys. Res. Lett., 25, 845
Stroman, T., Pohl, M., & Niemiec, J. 2009, ApJ, 706, 38
Vink, J. 2008, in AIP Conf. Ser. 1085, High Energy Gamma-ray Astronomy, ed. F. A. Aharonian, W. Hofmann, & F. Rieger (Melville, NY: AIP), 169
Vladimirov, A., Ellison, D. C., & Bykov, A. 2006, ApJ, 652, 1246
Völk, H. J., Berezhko, E. G., & Ksenofontov, L. T. 2005, A&A, 433, 229
Zirakashvili, V. N., Ptuskin, V. S., & Völk, H. J. 2008, ApJ, 678, 255